JOURNAL OF SOLID STATE CHEMISTRY **122,** 291–296 (1996)
ARTICLE NO. 0115

Mechanisms of Incipient Chemical Reaction between $Ca(OH)_2$ and SiO_2 under Moderate Mechanical Stressing

II: Examination of a Radical Mechanism by an EPR Study

Tomoyuki Watanabe, Tetsuhiko Isobe, and Mamoru Senna[1]

Faculty of Science and Technology, Keio University, 3-14-1 Hiyoshi, Yokohama 223, Japan

Received August 28, 1995; in revised form December 6, 1995; accepted December 12, 1995

An EPR spectroscopy was examined in detail in order to elucidate the role of mechanically induced radicals on the incipient mechanochemical reaction between $Ca(OH)_2$ and SiO_2. The specific radical species found on separately milled $Ca(OH)_2$ and SiO_2 disappeared in the case of mixed milling. O^- radicals on $Ca(OH)_2$ and E′centers on the SiO_2 surface reacted during milling, leading to a precursor of complex oxide with Si–O–Ca bonding. Relative contribution of radical mechanism was compared with those of electron pairs to the complex formation of Si–O–Ca under mechanical stressing.

1. INTRODUCTION

Electron paramagnetic resonance (EPR) spectroscopy has been extensively used to examine surface and bulk defects of various inorganic materials. For silica glasses, irradiation of γ ray (1, 2) or neutron (3) induces E′-center and peroxy radicals. CaO and $Ca(OH)_2$ were also studied by EPR. Surface radicals by adsorption of oxygen were found on thermally activated CaO (4). Irradiation of electron beams (5) and UV (6) is also known to generate oxygen radials, F center (electron trap by oxygen vacancy) or V center (positive hole trap by cation vacancy).

Mechanically induced radicals were studied by EPR, as well. For example, E′ centers are induced by scratching on the silicon {111} surface (7), mechanochemical activation leads to the production of triplet radical pairs of porphyrin and quinone (8), a trivalent titanium ion, Ti^{3+}, associated with oxygen vacancies on the surface of anatase is generated by milling (9), and E′ center increases by milling silica (10). Enhanced reactivity of MgO by milling has been understood as a consequence of oxygen-related radicals, e.g., F^+ center and O^- (11).

In our previous report (12), we have shown that mechanically induced reactive acidic and basic sites interact with each other. As a result, precursors of complex oxide, e.g., $CaSiO_3$, are formed. Avvakumov and co-workers have explained that the mechanochemical reactivity of binary systems depends on the difference between the acidity and basicity of the reactants (13). Up to now, the mechanism of mechanochemical synthesis has been discussed only on the basis of acid–base interaction, i.e., reactions by the change in the state of electron pairs.

In this paper, an EPR spectroscopy is used to examine whether and to what extent the mechanically induced radicals play a role on the mechanochemical reaction between $Ca(OH)_2$ and SiO_2. We also try to discuss the relative contribution of radicals to that of electron pairs (acid–base reaction) to the complex formation under mechanical stressing.

2. EXPERIMENTAL

$Ca(OH)_2$ was a guaranteed grade reagent (Wako Junyaku 99.9%). The specific surface area was 7.19 $m^2 \cdot g^{-1}$, determined by the N_2 BET method. Fumed silica powder (Degussa, Aerosil 200) was used as a silica source. One gram of sample in total was milled in air. Milling was then performed in vacuum as well to avoid the effects of the gaseous species in the ambient atmosphere. After evacuating a cylindrical PTFE container at room temperature for 1 h, mechanical activation was carried out at 10^{-1} Pa by a laboratory sized vibration mill (Glen-Creston, amplitude: 50 mm, frequency: 12 Hz). Activated samples were put into a quartz tube for EPR measurement without being exposed to air. EPR spectra were measured by an X-band spectrometer (JEOL JES-RE3X) at room temperature. Two resonance peaks at $g = 1.981$ (corresponding to 332 mT) and $g = 2.034$ (341 mT) due to Mn^{2+} contained as an impurity in $Ca(OH)_2$ were used as an internal standard for the calibration of applied magnetic field.

The mechanically activated samples are noted as follows.

[1] To whom correspondence should be addressed.

0022-4596/96 $18.00

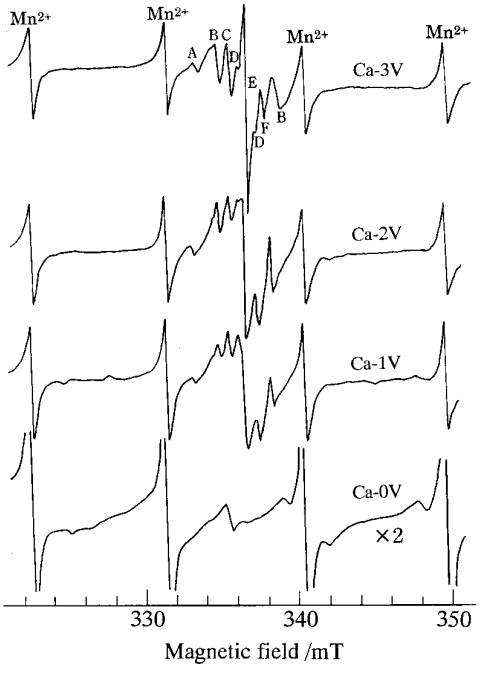

FIG. 1. EPR spectra of initial and separately milled $Ca(OH)_2$ at 4 mW microwave power, where *t* indicates the milling time in hours. The *g* values are A, 2.021; B, 2.014 and 1.991; C, 2.009; D, 2.005 and 1.999; E, 2.002; F, 1.996; respectively.

Ca and S denote $Ca(OH)_2$ and SiO_2, respectively, and -*t*, milling time in h throughout the figures. The additional symbol V denotes milling in vacuum. For the purpose of inducing well-defined defects, the powder $Ca(OH)_2$ was irradiated with X-ray produced by an Rh cathode tube operating at 50 kV and 40 mA, and then spectroscopy was carried out in the same manner. The microwave power saturation method was also used for the purpose of assignment of overlapping complex EPR signals.

3. RESULTS AND DISCUSSION

3.1. EPR Spectrograms of Milled and X-Ray Irradiated Ca(OH)$_2$

The EPR spectrogram for the samples of separately milled $Ca(OH)_2$ at 4 mW microwave power is shown in Fig. 1. After milling $Ca(OH)_2$ in vacuum, we observe very complicated EPR spectra. The peaks comprise six different components, denoted A to F. They are by no means attributed to some organic species possibly abraded from nylon coated balls and a PTFE vessel, since no such EPR signals are observed on silica separately milled for 3 h in air. Rather, the peaks A to F seem to be attributed to oxygen-related radicals including F^+ centers like those found on milled MgO by Steinike *et al.* (11).

For the purpose of identification of active centers on milled materials, we introduced a series of well-defined defects by an irradiation of X ray *in vacuo* on $Ca(OH)_2$, since there is a much smaller number of reports on the EPR signals from $Ca(OH)_2$, as compared with those from SiO_2 (10, 11). Apart from well-distinguished Mn peaks, we observe 2 small peaks at $g = 2.009$ (denoted by (1)) and $g = 2.068$ (2) on the intact $Ca(OH)_2$ as shown in Fig. 2. These are attributed to the V center, i.e., a positive hole entrapped at a Ca^{2+} cation vacancy (6, 14–16). The unpaired spins causing these resonance peaks are related with *p* electrons and hence are anisotropic. Peaks (1) and (2) are parallel and perpendicular components, respectively, of the V center.

On irradiation for 0.1 s, a weak spin (3) at $g = 2.002$ and a strong one (4) at $g = 1.999$ appear. These two peaks unify into one at $g = 2.000$ (peak (5)) on further irradiation. No changes on the EPR spectra are observed on prolonged X-ray irradiation. According to Matsuhashi *et al.* (17), there are two different F^+ centers generated on the unstable and stable surface spots, respectively. These F^+ centers have a strong tendency to donate an electron, enabling the catalysis of dehydrogenation of isopropyl benzene or hydrogenation of alkenes (17). Peaks (3) and (4) are likely to be the F^+ centers on metastable and stable areas, respectively. The *g* value of signal (3) generated by X-ray irradiation is similar to that of signal E induced by mechanical stressing in Fig. 1. The signals A, B, D, and F presented

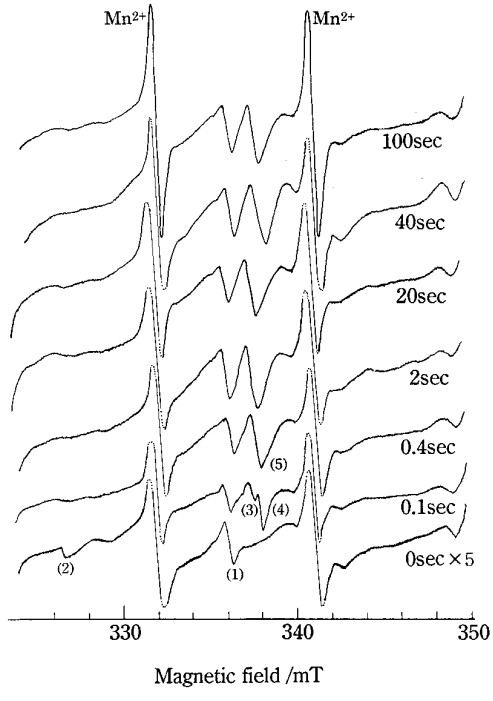

FIG. 2. EPR spectra of $Ca(OH)_2$ irradiated by X-ray for quoted time(s) at 4 mW microwave power. The *g* values; (1) $g = 2.009$, (2) $g = 2.068$, (3) $g = 2.002$, (4) $g = 1.999$, (5) $g = 2.000$.

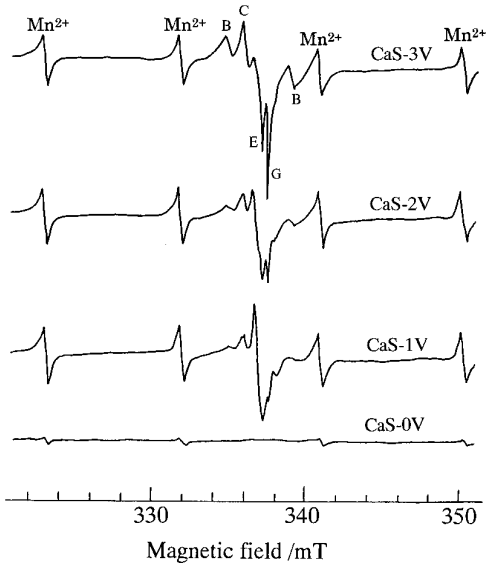

FIG. 3. EPR spectra of the initial and milled $Ca(OH)_2$–SiO_2 mixture, CaS-*t* at 4 mW microwave power. The *g* values are B, 2.014 and 1.991; C, 2.009; E, 2.002; G, 2.000; respectively.

on the separately milled $Ca(OH)_2$ are absent on the X-ray irradiated one. This will be further discussed in Section 3.2 by power saturation method.

3.2. Assignments for EPR Spectra of Milled Samples

EPR spectra at 4 mW microwave power of the mixed-milled sample is shown in Fig. 3. The spectra are similar to that of separately milled $Ca(OH)_2$ in Fig. 1. However, the signals A and F are absent and the signal G, due to the defects on SiO_2, is present in the case of the mixed-milled sample. The signals induced by X-ray irradiation to $Ca(OH)_2$ do not enable us to fully assign the complex signals of these milled samples. Therefore, a microwave power saturation method was employed.

As shown in Fig. 4, the dependence of the peak heights relative to their own maxima with the square root of microwave power for separately milled $Ca(OH)_2$ (Ca-3V in Fig. 1) are divided into three categories, (I)A, D, and F; (II)B and E; and (III)C. Knowing that all the signals but C in Fig. 1 change their intensity on exposure to ambient atmosphere, all others must be attributed to the surface defects and/or oxygen-related radicals. The signal C, being insensitive to the air exposure, might be related with bulk defects.

The *g* values of A and F signals are close to those of O_3^-, generated by a heat treatment of CaO, found by Cordischi *et al.* (4). The *g* value of D is close to that of CO_2^-, generated from He^+ and γ-ray irradiation on $CaCO_3$ (18). The power saturation behavior of A and F are also similar to those of O_2^- or O_3^-, identified by Giamello *et al.* (19) on MgO sputtered Mg thin film. The power saturation behavior of signal D is similar to that of CO_2^- (18). O_2^- is formed by a single electron transfer to an oxygen molecule, while the formation of O_3^- is explained by the adsorption of an oxygen molecule on the O^- anion radical.

It is also to be noted that the intensity of signals A and F decreases relative to that of Mn after air exposure. Based on these changes, together with the comments given by Cordischi *et al.* (4) that the O_3^- radicals are very unstable and are easily deactivated, e.g., by the presence of H_2–O_2 gas mixture, we conclude that signals A and F are attributed to O_3^- radicals while signal D is attributed to CO_2^-. The latter radical sites are called as reducing sites. An electron transfer to adsorbed nitrobenzene at the reducing sites was detected by EPR (20). Such an electron transfer is easier when the spin is associated with low-coordinated surface oxygen atoms (21). The resulting O^- anion radicals are highly reactive and often coupled with a luminescence source (22).

On the other hand, signals B and E increase at relatively low microwave intensity, with a gradual decrease on further increase in the microwave power. This is quite similar to the behavior of the F^+ center, as detected from alkali metals like Li or Na sputtered on MgO (17, 23) or Mg (19). The *g* value of the signal E is close to that of the F^+ center induced by X-ray irradiation, as referred to in the Section 3.1. Signals B and E are, therefore, likely to be attributed to the F^+ centers. The broadness of signal B could be explained by assuming the interaction of the electrons entrapped at the oxygen vacancy with hydrogen atoms of the hydroxyl groups (19, 24), whose energy state is widely distributed. Finally, signal C, being invariant to

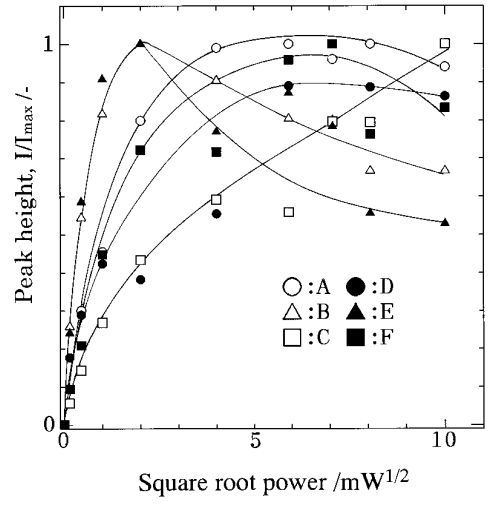

FIG. 4. Peak height (in arbitrary units) versus the square of the microwave power for the A–F paramagnetic species observed for Ca-3V in Fig. 1.

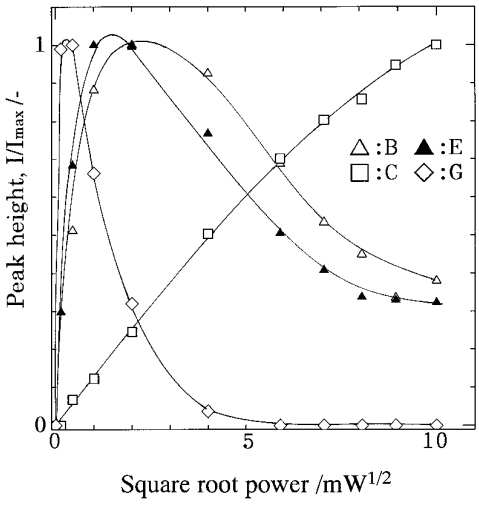

FIG. 5. Peak height (in arbitrary units) versus the square of the microwave power in mixed-milled sample (CaS-3V in Fig. 3).

air exposure, must be associated with bulk defects, e.g., V centers.

Power saturation behavior of the spins detected from the mixed-milled samples are shown in Fig. 5. While the shape of curves of B, C, and E are similar to those of separately milled samples shown in Fig. 4, the change of signal G is quite unique and is solely to be observed on the mixed-milled sample. From the g value and its power saturation behavior (1, 3, 10), signal G is suspected to be an E′center in SiO_2.

Figure 6 shows EPR spectra of separately milled SiO_2 at 0.02 mW microwave power, and the power saturation curves are shown in Fig. 7. From the examination of the powder saturation behavior shown in Fig. 8 and based on the information given in Ref. (1, 3, 10, 25), signal G is again confirmed to be the E′ center ($\equiv Si\cdot$) in SiO_2, whereas signal H is confirmed to be the peroxy radical (POR; $\equiv Si–O–O\cdot$), i.e., molecular oxygen at defect sites (E′ center). The E′ center, i.e., signal G, is also present in the mixed-milled sample in Fig. 3. Since signal I appeared in a lower magnetic field than those of E′ and POR centers, the signal is likely to be attributed to nonbridging oxygen hole center (NBOHC; $\equiv Si–O\cdot$) (25).

3.3. Difference in the Radicals Induced by Separate and Mixed Milling

The main differences between separately milled $Ca(OH)_2$ (Fig. 1) and mixed-milled samples (Fig. 3) are (i) the absence of signals A and F due to O_3^- radicals on the mixed milled samples, and (ii) the opposite change of signal E due to F^+ center with milling time, an increase on separate milling versus a decrease on mixed milling. Point (i) is explained by the coexistence of silica, as will be discussed later below.

F^+ centers are formed only after milling. As a result of mechanochemical dehydration, oxygen vacancy will be formed when a proton necessary for dehydration is supplied from the hydroxyl groups belonging to the hollow site type (26). This suggests easier formation of the F^+ center for the condition leading to easier mechanochemical

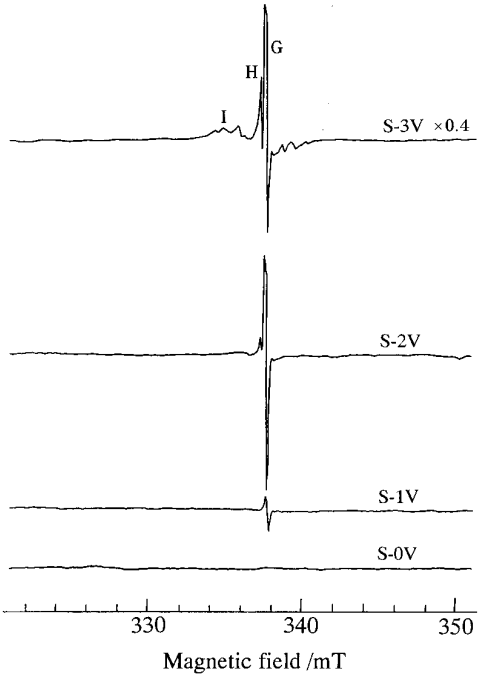

FIG. 6. EPR spectra of initial and separately milled SiO_2 at 0.02 mW microwave power. The g values are G, 2.000; H, 2.001; I, 2.003.

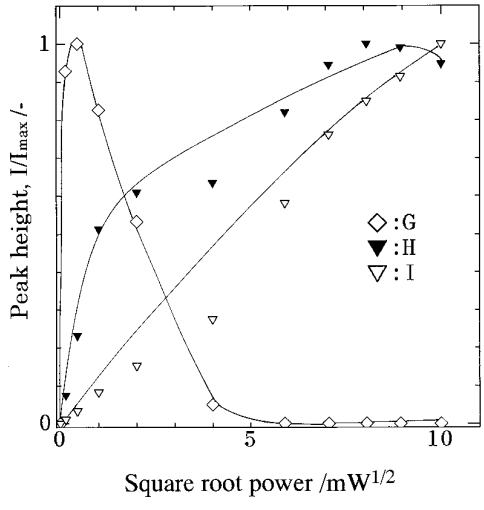

FIG. 7. Peak height(in arbitrary units) versus the square of the microwave power in separately milled SiO2 in vacuum (S-3V in Fig. 6).

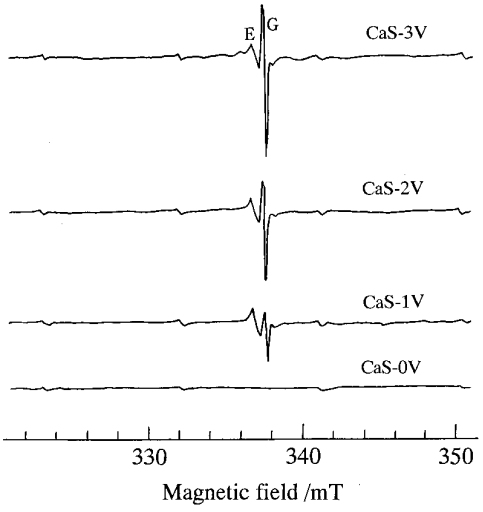

FIG. 8. EPR spectra of the initial and milled $Ca(OH)_2$–SiO_2 mixture at 0.02 mW microwave power. The *g* values are G, 2.000 and E, 2.002.

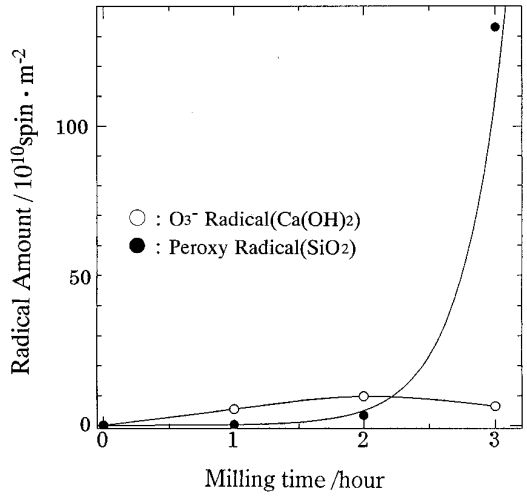

FIG. 10. Variation of radical concentration in separately milled samples with milling time.

dehydration (12, 26–28). This is quite compatible with the observation that the formation of the F^+ center on mixed milling is faster than on separate milling, judging from the comparison between Figs. 1 and 3. The electron entrapped by surface oxygen vacancy could survive when only one kind of cation exists as in the case of separate milling. It transfers from the F^+ center to the different cations, Si, when those with higher electron affinity coexist. The latter is the case of mixed milling. Thus, the easier mechanochemical dehydration is explained not only by the acid–base reaction reported previously (12) but also by the radical mechanism mentioned above.

Comparison of milling silica separately and with $Ca(OH)_2$ brings about another aspect of the radical mechanism. As shown in Figs. 3 and 6, the E′ and POR centers, denoted by signal G and H, respectively, generated in separately milled SiO_2 are hidden by the large signals in mixed-milled samples. To further examine the argument, EPR signals were measured for mixed-milled samples under still lower microwave power, 0.02 mW, because, as shown in Figs. 5 and 7, the E′ center is not saturated yet at this power. As shown in Figs. 6 and 8, signal G, being attributed to E′ centers, increased in both cases. At the same time, signal H, being attributed to POR centers, increased only in the case of the separately milled SiO_2, and are not detected at all in the case of mixed milling. The POR center is formed by the oxygen adsorption to the E′ center (25); it takes place as long as other cationic species are absent. This supports the idea that the surface E′ centers, leading to the formation of POR centers, are consumed by the interaction with the radicals presented on the $Ca(OH)_2$.

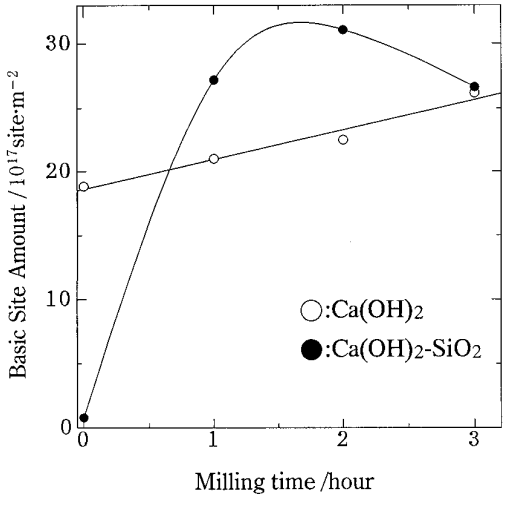

FIG. 9. Changes in the surface basicity of $Ca(OH)_2$ and $Ca(OH)_2$–SiO_2 due to mechanical activation.

3.4. Mechanisms of Radical Reactions

One of the most remarkable differences between separated and mixed milling (Figs. 1 and 3) is a disappearance of O_3^- species, denoted by A and F, in the case of mixed milled CaS-3. The absence of these signals is linked with the absence of POR (signal H) in Fig. 8, in contrast to survival of this radical species in the separately milled samples, as shown in Fig. 6. The difference could be interpreted by the following scheme of radical recombination:

$$\mathrm{Ca(OH)_2{:}\ OH^- + OH^- \xrightarrow{\text{mechanical dehydration}} H_2 + O^- + O^-(Ca{-}O\cdot)} \xrightarrow[\text{oxygen adsorption}]{} \mathrm{H_2 + O_3^-\ (signal\ A\ and\ F).} \quad [1]$$

These oxygen radicals can be formed even if mechanochemical dehydration takes place simultaneously. Meanwhile, the peroxy radicals can be formed by the following reaction scheme:

$$\mathrm{SiO_2}: \equiv \mathrm{Si{-}O{-}Si} \equiv \xrightarrow{\text{mechanical activation}} \equiv \mathrm{Si{-}O}\cdot + \equiv \mathrm{Si}\cdot \xrightarrow{\text{oxygen adsorption}} \equiv \mathrm{Si{-}O}\cdot\ (\text{signal I}) + \equiv \mathrm{Si{-}O{-}O}\cdot\ (\mathrm{H}). \quad [2]$$

Since oxygen adsorption is a prerequisite for POR formation, E′ centers must be located on the surface, together with the O_3^- on the surface of $Ca(OH)_2$. When the radical species generated in schemes' [1] and [2] first steps react with each other, they are annihilated by the scheme

$$\mathrm{Ca(OH)_2{-}SiO_2}: \mathrm{Ca{-}O}\cdot + \equiv \mathrm{Si}\cdot \xrightarrow{\text{radical recombination}} \mathrm{Ca{-}O{-}Si} \quad [3]$$

3.5. Relative Role of Electron Pair and Radical Mechanisms

At the end of the present study on the radical mechanism, we discuss quantitatively the relative contribution of the acid–base reaction as an electron pair mechanism and the radial mechanism discussed extensively in the foregoing. The concentration of surface basicity is cited from our previous report (12) as Fig. 9. This is now compared with the surface concentration of the radical, determined with the aid of the radical standard, TEMPOL (4-hydroxy-2,2,6,6-tetramethyl-1-piperidine-1-oxyl). The result is shown in Fig. 10. The basic site concentration on the surface is six to seven orders of magnitude higher than the radical concentration. It seems therefore clear that the relative role of the electron pair mechanism is by far larger than that of the radical mechanism. The statement is to be understood with care, however, since the comparison of the concentration does not account for the kinetic factors, for which radical mechanisms could well conquer the electron pair mechanism, because of the rapid radical recombination involved. Further studies are therefore necessary for the comprehensive discussion with regard to the relative contribution of electron pair and radical mechanisms.

4. CONCLUSION

During mechanochemical complex formation between $Ca(OH)_2$ and SiO_2, various species of radicals are formed as a result of dehydration and various kinds of bond breakage. O^- radicals on $Ca(OH)_2$ and E′ centers on SiO_2 can react during milling, leading to a complex Si–O–Ca bonding, and annihilate by each other. The relative importance of radical mechanisms seems, however, to be smaller than the electron pair mechanism represented by an acid–base reaction.

REFERENCES

1. W. Chamulitrat, L. Kevan, R. N. Schwartz, G. Richard, and G. L. Tangonan, *J. Appl. Phys.* **59,** 2933 (1986).
2. R. A. B. Devine, *J. Non-Cryst. Solids* **107,** 41 (1988).
3. M. Ikeya, H. Kohno, S. Toyoda, and Y. Mizuta, *Jpn. J. Appl. Phys.* **31,** 1539 (1992).
4. D. Cordischi, V. Indovina, and M. Occhiuzzi, *J. Chem. Soc. Faraday. Trans. 1* **74,** 883 (1978).
5. J. Marks, W. T. Wenckebach, and N. J. Poulis, *J. Phys. C: Solid State Phys.* **13,** 5481 (1980).
6. Y. Yanagisawa, N. Inishi, and A. Narumi, *Phys. Rev. B* **46,** 11121 (1992).
7. Y. Saito, T. Isobe, and M. Senna, *J. Solid State Chem.* in press.
8. S. D. Chemerrisov, O. Y. Grinberg, D. S. Tipikin, Y. S. Lebedev, H. Kurreck, and K. Mobius, *Chem. Phys. Lett.* **218,** 353 (1994).
9. J. M. Criado, C. Real, and J. Soria, *Solid State Ionics* **32–33,** 461 (1989).
10. T. Fukuchi, *Appl. Radiat. Isot.* **44,** 179 (1993).
11. U. Steinike, U. Kretzschmar, I. Ebert, H. P. Henning, L. I. Barsova, and T. K. Jurik, *React. Solids* **4,** 1 (1987).
12. T. Watanabe, J. Liao, and M. Senna, *J. Solid State Chem.* **115,** 390 (1995).
13. E. G. Avvakumov, E. T. Devyatkina, and N. V. Kosova, *J. Solid State Chem.* **113,** 379 (1994).
14. Yu. I. Aristov, V. N. Parmon, and K. I. Zamaraev, *React. Kinet. Catal. Lett.* **27,** 245 (1985).
15. T. P. P. Hall, *J. Phys. C: Solid State Phys.* **8,** 1921 (1975).
16. M. M. Abraham, Y. Chen, L. A. Boatner, and R. W. Reynolds, *Solid. State. Commun.* **16,** 1209 (1975).
17. H. Mastubashi, T. Hasegawa, M. Okuyama, and K. Arada, *Shokubai* **35,** 364 (1993).
18. H. Kohno, C. Yamanaka, M. Ikeda, S. Ikeda, and Y. Hirono, *Nucl. Instrum. Meth. Phys. Res. Sec. B* **91,** 366 (1994).
19. E. Giamello, A. Ferrero, S. Coluccia, and A. Zecchina, *J. Phys. Chem.* **95,** 9385 (1991).
20. T. Iizuka, H. Hattori, Y. Ohno, J. Sohma, and K. Tanabe, *J. Catal.* **22,** 130 (1971).
21. T. Ito, *Hyomen Kagaku* **8,** 488 (1987).
22. O. C. Plucher and J. C. Niepce, *J. Mater. Sci. Lett.* **6,** 1231 (1987).
23. D. Murphy, E. Giamello, and A. Zecchina, *J. Phys. Chem.* **97,** 1739 (1993).
24. A. J. Tench and R. L. Nelson, *J. Collid Interface Sci.* **26,** 364 (1968).
25. D. L. Griscom, *J. Ceram. Soc. Jpn.* **99,** 923 (1991).
26. T. Watanabe, T. Isobe, and M. Senna, *J. Solid State Chem.* in press.
27. J. Liao and M. Senna, *Solid State Ionics* **66,** 313 (1993).
28. E. G. Avvakumov, *Chem. Sustainable Dev.* **2,** 1 (1994).